Journal of Power Sources 196 (2011) 2595–2601

Contents lists available at ScienceDirect

Journal of Power Sources

journal homepage: www.elsevier.com/locate/jpowsour

Activation of dispersed PtSn/C nanoparticles by tungsten oxide matrix towards more efficient oxidation of ethanol

Krzysztof Miecznikowski, Pawel J. Kulesza*

Department of Chemistry, University of Warsaw, Pasteura 1, PL-02-093 Warsaw, Poland

ARTICLE INFO

Article history:
Received 19 August 2010
Received in revised form 8 October 2010
Accepted 23 October 2010
Available online 9 November 2010

Keywords:
Fuel cells
PtSn/C nanoparticles
Tungsten oxide
Ethanol oxidation
Electrocatalysis
Carbon monoxide

ABSTRACT

A novel electrocatalytic system for oxidation of ethanol, in which carbon-supported PtSn nanoparticles were modified with ultra-thin films/deposits of tungsten oxide, was proposed, fabricated and characterized here using electrochemical as well as spectroscopic (X-ray diffraction) and microscopic (transmission electron) techniques. The enhancement effect was evident from comparative diagnostic electrochemical experiments utilizing WO_3-modified and bare (unmodified) PtSn nanoparticles in acid medium (0.5 mol dm^{-3} H_2SO_4) at room temperature in the presence of ethanol. It is noteworthy that, the chronoamperometric electrocatalytic currents measured at potentials as low as 0.3 V (vs. RHE) were significantly larger for WO_3-modified PtSn/C relative to bare PtSn/C. In another diagnostic "stripping" experiment, it was found that oxidation of CO-adsorbate occurred in the presence of WO_3 at potentials almost 100 mV lower in comparison to the unmodified system. The overall activation effect may have origin in interactions of tungsten oxide with tin (from PtSn alloy nanoparticles) leading to stabilization of the catalytic tin oxo species. WO_3 may also provide large population of reactive oxo groups at the Pt/Sn-based electrocatalytic interface.

1. Introduction

Recently, there has been growing interest in development of the direct alcohol fuel cells (DAFCs) as alternative technology to hydrogen based electrochemical energy systems. Alcohols have several potential advantages in comparison to the hydrogen: relatively low cost of production, simplicity in handling, storage and transport, as well as high solubility in aqueous solutions. Among small organic molecules, ethanol, being a renewable biofuel, is a promising candidate for a fuel cell. In the case of ethanol, a catalyst that could efficiently convert the substrate to carbon dioxide would produce a fuel cycle capable of delivering theoretically 12 electrons; and the cell could yield a theoretical open circuit potential of 1.14 V. Unfortunately, the splitting step of the C–C bond (in ethanol molecule) that is required for its complete oxidation to CO_2 is a major mechanistic limitation during the electrocatalytic reaction. Consequently, large amounts of partial oxidation products, such as CH_3CHO and CH_3COOH (rather than CO_2) are formed at Pt-based catalysts [1–3]. These parallel reactions cause considerable problems in practical applications of DAFCs not only by lowering the fuel capacity but also by producing undesirable toxic by-products. Recent attempts to develop means of photoelectrochemical degradation of the ethanol oxidation intermediates [4] should be mentioned here.

Nanostructured platinum is so far the best-known and the most active catalyst for the activation of small organic molecules via their specific adsorption and interfacial dissociation [5]. However, the ability of platinum to break effectively the C–C bonds is largely limited by side poisoning effects originating from the strong adsorption of CO_{ads} on Pt surfaces at low (below 60 or even 80 °C). Several two-carbon containing molecules have been reported as undesirable intermediates during ethanol oxidation at polycrystalline Pt [6–8], most of them requiring relatively high potentials for complete oxidation [7]. It has also been suggested that the partial blocking of platinum surface by those intermediates results in slow decay with time of the ethanol oxidation currents [9].

The problem of CO-poisoning during electrooxidation of methanol has been largely overcome by alloying Pt, adding to it, or by modifying the metal with some ruthenium. Ruthenium may activate molecules of water and create the adsorbed –OH groups capable of removing of CO adsorbates through interfacial electrooxidation to CO_2 [10–13].

For ethanol, the mechanism of its electrooxidation is different and more complex than in a case of methanol. It is commonly accepted that the highest efficiency for electrooxidation of ethanol was achieved at carbon-supported PtSn (PtSn/C) catalysts [14–17] and, more recently, very promising result were obtained with PtRh type systems [18,19]. Despite the relatively good performance of

* Corresponding author. Tel.: +48 8220211x289; fax: +48 8225996.
E-mail addresses: kmiecz@chem.uw.edu.pl (K. Miecznikowski), pkulesza@chem.uw.edu.pl (P.J. Kulesza).

0378-7753/$ – see front matter © 2010 Elsevier B.V. All rights reserved.
doi:10.1016/j.jpowsour.2010.10.078

the PtSn/C based anodes, the overall efficiency is still poor when compared to oxidation of hydrogen (at Pt) or even methanol (at PtRu) [14]. The main products remain acetaldehyde (2-electron oxidation) and acetic acid (4-electron oxidation) thus further modification of existing catalysts is necessary to obtain higher efficiency. There is a need to remove not only the poisoning CO adsorbates but also to activate the ethanol molecule and to break C–C bonds effectively. Often modification of the platinum-based surface is achieved by adding the second additive namely by introducing the second alloying metal [1,20–22]. As a third metal in PtSn catalysts, ruthenium [17], iridium [23], and tungsten [24,25] have been considered. More recently, it has been demonstrated that the presence of WO_x increases the electrochemical activity of PtRu catalyststoward ethanol oxidation [26] in terms of higher electrocatalytic current densities and lower potential values. Ternary PtSnW catalysts prepared by thermal decomposition of polymeric precursor and their application in the ethanol electro-oxidation have also been studied [24]. Tungsten is known to promote Pt in different oxidation processes because tungsten oxides tend to interact with CO adsorbates on the Pt surface [27–29].

In the present paper we have studied the influence of tungsten oxide (WO_3•H_2O or H_2WO_4) on the catalytic activity of PtSn/C systems towards electrooxidation of ethanol. WO_3 was reported to act not only as powerful electroreduction catalyst for such inert reactants as oxohalogenates or hydrogen peroxide [27–31] but also as the electrooxidation catalyst for CO [26,32,33]. WO_3 was demonstrated to promote electrocatalytic oxidation of methanol by interacting with Pt via hydrogen spillover or through the formation of highly conductive tungsten bronzes [27]. Other important properties of tungsten oxide films included high rates of charge (electron and proton) propagation [29,34–36] and ability to transfer electrons effectively to three-dimensionally distributed catalytic centers [27,37,38]. On the whole, the activating role of tungsten oxide may be due to the presence of OH_{ads} groups on the oxide surface that should facilitate oxidation of poisoning CO intermediates [32], the increase of the electrochemically active surface area [39], and the existence of the hydrogen spillover effect at the interface between platinum and WO_3 [27,40]. Here we have found that WO_3-modified

PtSn/C nanoparticles exhibit superior electrocatalytic activity towards electrooxidation of ethanol in comparison to bare (unmodified) catalyst.

2. Experimental

All chemicals were commercial materials of analytical grade purity. PtSn/C nanoparticles (20% on Vulcan, Pt:Sn 3:1) were obtained from E-TEK. Solutions were prepared using doubly-distilled and subsequently de-ionized (Millipore Milli-Q) water. Argon was used to de-aerate solutions and to keep the air-free atmosphere over the solution during the measurements. The morphology of catalytic particles was monitored using a JEOL 200 CX transmission electron microscope (TEM) operating at 200 kV. Samples for TEM measurements were prepared by placing of colloidal solutions of nanoparticles on Formvar film grids (Agar Scientific) and, later, by subjecting them to drying on the 400 mesh Cu. X-ray diffraction (XRD) patterns of the catalysts were obtained on Bruker D8 Discover operating with a Cu lamp (1,54 Å) and Vantec (linear) detector (k = 1.5406 Å).

All electrochemical measurements were performed using CH Instruments 750 A workstations in three electrodes configuration. The reference electrode was the K_2SO_4-saturated Hg_2SO_4 electrode, and the carbon rod was set as a counter electrode. All potentials in the present work were recalculated and expressed versus reversible hydrogen electrode (RHE). Glassy carbon served as the working electrode, onto which inks of PtSn/C nanoparticles were immobilized. The solution of tungstic acid was obtained by passing an aqueous 0.05 mol dm^{-3} Na_2WO_4 solution through a proton exchange resin, Dowex 50 WX2-200. The suspension of Vulcan-supported PtSn nanoparticles (PtSn/C) was prepared as follows: a known amount (10 mg) of PtSn/C nanoparticles was dispersed in 2 cm^3 of 0.05 mol dm^{-3} aqueous solution of tungstic acid. The suspension was mixed using magnetic stirring for 24 h and centrifuged. Then supernatant solution was replaced with water, and the stable suspension of WO_3-modified PtSn/C nanoparticles was produced. The approximate molar ratio of Pt to tungsten oxide was 1:1. To immobilize catalytic nanoparticles, 6 μl aliquot of the suspensions was dropped using micropipette on the glassy carbon electrode surface. The resulting layer was left for 30 min to dry at room temperature. Then 2 μl of Nafion (0.02% alcoholic solution) was dropped on top of the glassy carbon electrode surface covered with the catalyst. The Nafion film was sufficiently stable to fix the modified and unmodified catalytic nanoparticles on the electrode substrate in the supporting electrolyte. As a rule, the catalytic electrodes were conditioned through application of 25 complete oxidation/reduction cycles at 50 mV s^{-1} between 0 and 0.8 V in 0.5 mol dm^{-3} H_2SO_4. The total loading of PtSn nanoparticles was approximately 160 μg/cm^2.

The CO-stripping measurements were performed in 0.5 mol dm^{-3} H_2SO_4 electrolyte using the glassy carbon electrode substrate onto which surface the appropriate catalyst was introduced. The electrolyte was first de-oxygenated by purging argon for 30 min. Subsequently, a few consecutive voltammetric scans (at 50 mV s^{-1}) were recorded in the potential range from 0.0 to 0.8 V. To saturate the solution with CO gas, pure CO (from Air Liquide) was bubbled through the electrolyte for 10 min. The actual CO-adsorption step (on the surface of catalytic Pt nanocenters) was achieved upon application of the potential of 0.1 V for 5 min after which the electrolyte was purged with argon for 30 min under open-circuit conditions to remove dissolved CO. As a rule, three cyclic voltammetric scans (at 10 mV s^{-1}) were recorded in the potential range from 0.0 to 0.9 V. Most of the experiments using these catalysts were reproduced two to three times with freshly prepared electrodes to ensure the reproducibility of electrode preparation and performance.

3. Results and discussion

Fig. 1 shows TEM images of (A) PtSn/C and (B) WO_3-modifed PtSn/C catalytic nanoparticles. Low-magnification images show that approximately spherical bimetallic nanoparticles are in both cases uniformly dispersed on the surfaces of carbon (Vulcan XC-72R) supports, and the distribution lies in a narrow particle size range. The histograms of the particle size distribution (Fig. 1), which reflect analyses of several different portions of the catalysts, are also consistent with the uniform distribution in these catalysts. The sizes of PtSn particles were between 2 and 6 nm, with a mean diameter of 4 nm, which well agrees with the value of the crystallite size of the PtSn/C calculated by XRD. The sizes of WO_3-modifed PtSn/C particles were comparable, and they lied between 3 and 6 nm having a mean diameter of 4.5 nm (Fig. 1). Some increase in the particle size is probably due to the adsorption of WO_3 on the PtSn/C phase. High magnification TEM micrographs (Fig. 1) reveal the asymmetric faceted shape, typically cubooctahedral, of PtSn.

Fig. 2 illustrates the XRD patterns of the carbon supported PtSn and WO_3-modifed PtSn catalysts. The diffraction peak at 20–25° observed in all the XRD patterns of the carbon-supported catalysts is due to the (0 0 2) reflection of the hexagonal structure of Vulcan XC-72 carbon. The main characteristic peaks of the face-centered cubic crystalline Pt appear in all the patterns. The diffractogram

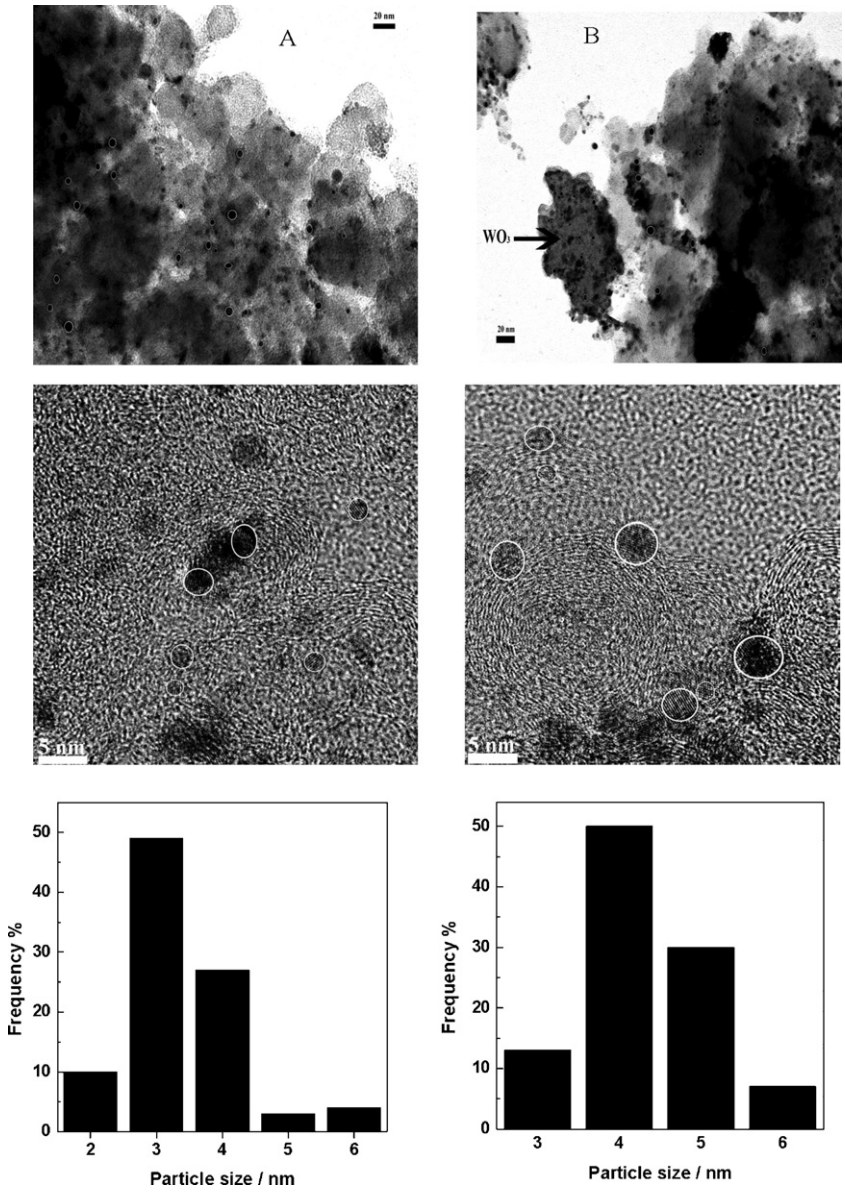

Fig. 1. Low-magnification and high-magnification micrographs (TEM) of PtSn/C (a), and WO_3-modifed PtSn/C (b) nanoparticles.

of the WO_3-modified PtSn/C electrocatalyst shows peaks at about $2\theta = 27$, 34, 52, 54, 62 and 66° that are associated with the (1 1 0), (1 0 1), (2 1 1), (2 2 0), (3 1 0) and (3 0 1) reflections, respectively, characteristic of cassiterite SnO_2 phase. In a case of WO_3-modifed PtSn catalysts, the signals characteristic of WO_3 are clearly visible in the XRD pattern (namely between $20° < 2\theta < 35°$). The WO_3 phase has characteristic peaks attributable to monoclinic WO_3.

The (2 2 0) reflections of Pt are used to calculate the average particle size according to the Scherrer equation:

$$L = \frac{0.9\lambda_{K\alpha 1}}{(B_{2\theta}\cos\theta_B)}$$

where L is the average particle size, $\lambda_{K\alpha 1}$ is the X-ray wavelength (1.54056 Å for Cu Kα1 radiation), $B_{2\theta}$ is the peak broadening and θ_B is the angle corresponding to the peak maximum. An expanded view of the (2 2 0) reflections of the fcc phase is shown in Fig. 2. The average Pt particle sizes obtained from XRD measurements was on the level 4–5 nm. The values of the average particle sizes obtained using TEM analysis are in good agreement with those calculated from the XRD results. As expected for alloyed Pt-based nanoparticles, the peak position at 40° was slightly shifted to lower 2θ values when compared to the literature data for pure Pt XRD pattern [25,26].

3.1. Electrochemical characterization of the catalysts

Preliminary diagnostic experiments involved cyclic voltammetric monitoring of the Nafion-treated pure (unmodified) PtSn/C and WO_3-modified PtSn/C nanoparticles deposited on glassy carbon in the deaerated supporting electrolyte of 0.5 mol dm^{-3} H_2SO_4. Typical results are presented in Fig. 3. The voltammograms display well-defined peaks in the hydrogen adsorption/desorption region (0.0–0.4 V) as well as typical currents in the double layer region between 0.4 and 0.9 V. This behavior is characteristic of carbon supported binary electrocatalysts containing transition metals [23]. It is not surprising that in a case of WO_3-modifed PtSn/C electrocatalysts, the presence of WO_3 leads to increase of the voltammetric hydrogen adsorption and desorption peaks due to so called hydrogen spillover effect. In other words, there is only an indirect proof for the existence of WO_3 because it is difficult to distinguish contri-

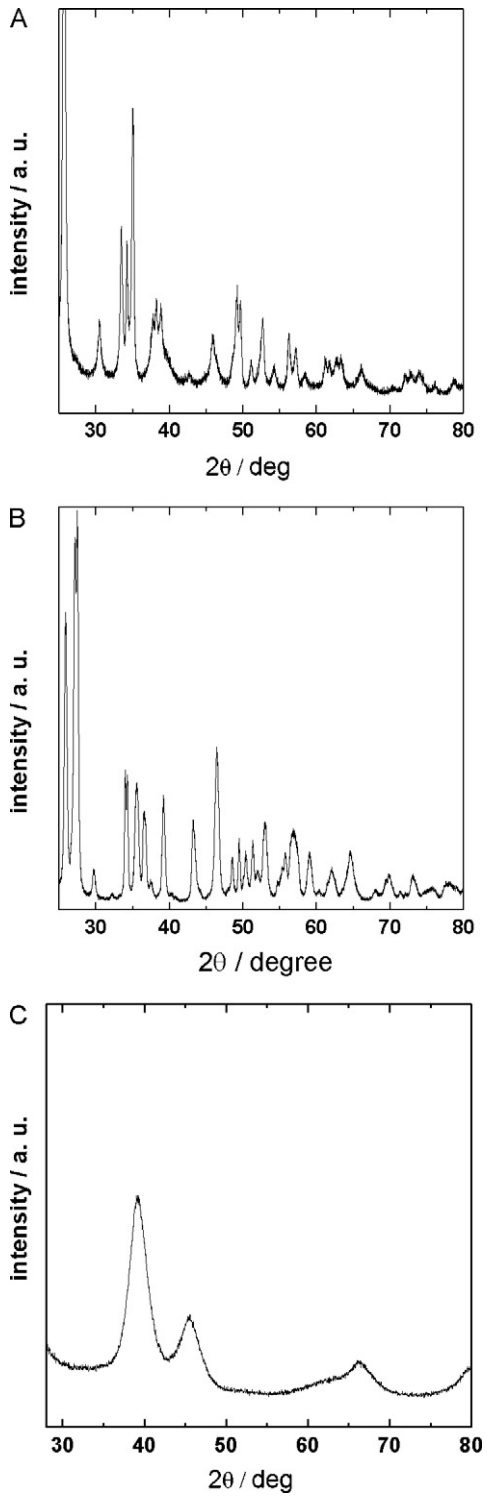

Fig. 2. XRD diffractograms of WO_3-modifed PtSn/C (a), WO_3 (b), and PtSn/C (c).

bution from the reversible reduction of tungsten oxide to hydrogen tungsten bronzes [27,28] from the above mentioned hydrogen adsorption and desorption peaks characteristic of Pt. Nevertheless, the peak appearing at about 0.05 V (Fig. 3, curve b) most likely reflects electroactivity of WO_3. Partial reduction of hydrated WO_3 leads to the formation of hydrogen tungsten oxide bronzes, H_xWO_3, that undergo fast reversible redox reactions

$$WO_3 + xH^+ + xe^- = H_xWO_3 (0 < x < 1)$$

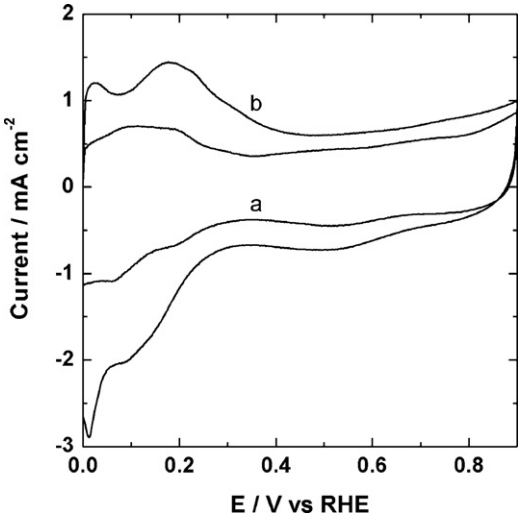

Fig. 3. Cyclic voltammetric responses of PtSn/C (a), and WO_3-modifed PtSn/C (b) catalytic systems in 0.5 mol dm^{-3} H_2SO_4. Scan rate: 10 mV/s.

overlapping and interacting with hydrogen adsorption/desorption peaks on platinum.

3.2. CO_{ads} stripping voltammograms in Ar-saturated electrolyte

The CO stripping voltammetric method was used here to comment of the ability of CO_{ads} poisoning-species to undergo oxidative desorption from the surface of PtSn/C in the presence of the tungsten oxide. Fig. 4 compares the base and the CO_{ads}-stripping voltammograms recorded for the bare (tungsten oxide-free) PtSn/C system (curve a) and for the WO_3-modifed PtSn/C (curve b). The upper potential limit was chosen to avoid the surface over-oxidation and irreversible damage to the electrocatalyst structure. The differences between the onset potentials for CO oxidation during the first anodic cycles recorded using WO_3-modified (solid line) and WO_3-free (dotted line) systems were shown in Fig. 4. In both cases, the CO-stripping (oxidation) peak appeared in the potential range from 0.35 to 0.85 V only during the first anodic cycle what meant that all adsorbed CO was oxidized under such conditions.

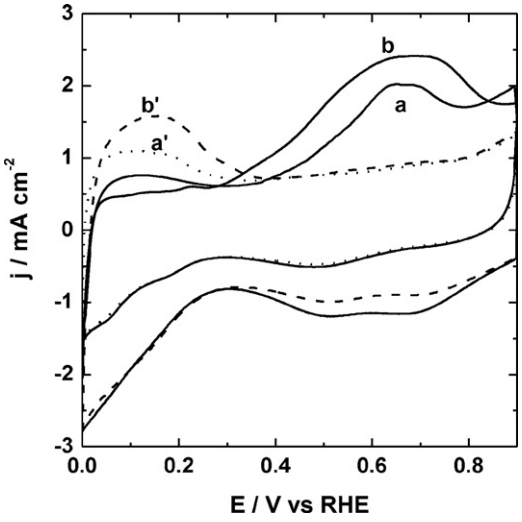

Fig. 4. CO stripping voltammograms recorded at 10 mV s^{-1} in 0.5 mol dm^{-3} H_2SO_4 for the PtSn/C (a), and WO_3-modifed PtSn/C (b) catalysts. CO adsorption was done at 0.1 V. Curves a and b show the first cycles while the curves a′ and b′ show the second cycles.

In other words, the CO-oxidation peak disappeared in the second anodic cycle. For the both catalysts, the CO oxidation peaks were significantly broadened and split into two peaks in comparison to simple Pt/C [41,42]. It is reasonable to correlate the peak appearing at the higher potential (ca. 0.70 V) to the oxidation of CO on Pt. On the other hand, the peak observed at the lower potential (in the range from 0.25 to 0.65 V) most likely originates from the oxidation of CO on Pt sites located close to the interface formed with the adjacent tin/tin oxide alloying component. The obtained results were in agreement with the previous reports [43,44] including PtMo alloys [45]. What is more important is that the addition of the tungsten oxide resulted in shifting of the onset potential for CO oxidation towards more negative values (Fig. 4). It was postulated that tungsten oxide induced oxidative removal of poisoning CO_{ads} species from Pt surface [27,32,33] via the bifunctional mechanism [46–48] proposed for Ru-oxo species. Having in mind recent high-resolution XPS studies describing interactions of PtSn with polyoxometallates [52], tungsten oxide is also expected to interact with tin (from PtSn alloy nanoparticles) through stabilization of the catalytic tin oxo species in addition to the postulated ability of WO_3 to provide large population of reactive oxo groups at the catalytic interface [32].

3.3. Ethanol electrooxidation

Fig. .5 illustrates the representative cyclic voltammograms obtained with PtSn/C and WO_3-modifed PtSn/C electrocatalysts deposited on glassy carbon electrode in the presence of 0.5 M ethanol in 0.5 M H_2SO_4 aqueous solution. The shapes of curves are typical for the electro-oxidation reactions of simple organic alcohols, showing two anodic peaks in the forward scan and in the reverse scan, respectively. They are related to the voltammetric oxidation of alcohol in the positive sweep as well as to the oxidation of incompletely oxidized carbonaceous species during the negative sweep. Ethanol electrooxidation starts ca. 100 mV earlier for WO_3-modifed PtSn/C in comparison to bare PtSn/C electrode, as can be seen in Fig. 5. Hydrogen adsorption/desorption peaks are largely decreased because adsorption of ethanol (or its oxidation intermediate by-products) suppresses formation of hydrogen peaks at the interface. On the other hand, all WO_3-modifed PtSn/C examined electrodes exhibited higher (certainly not lower) voltammetric electrocatalytic currents during oxidation of ethanol at the potentials lower than 0.5 V, i.e. in the potential range crucial from the viewpoint of potential application in fuel cells. The presence of WO_3 can be interpreted in terms of activation of interfacial water molecules at potentials lower to those expected for bare PtSn/C.

Fig. 6 illustrates background-subtracted linear scan voltammograms of PtSn/C (curve a) and WO_3-modifed PtSn/C (curve b) nanoparticles deposited on glassy carbon substrate recorded in the electrolyte of 0.5 M H_2SO_4 containing 0.5 M ethanol. The onset potentials for bare PtSn/C nanoparticles and for the WO_3-modifed PtSn/C catalyst were 0.29 V and 0.16 V, respectively. In the potential range, 0.3–0.4 V, the increase of current density for PtSn/C was less pronounced in the presence of ethanol when compared to the analogous measurement performed at WO_3-modifed PtSn/C nanoparticles. It is not clear whether WO_3 activates Pt or Sn/SnO_x sites at potentials lower than 0.45 V. The positive effect of Sn/SnO_x itself in the case of PtSn/C catalysts on the oxidation of ethanol has been reported by many groups [9,49,50], and it is usually explained in terms of supplying oxygen-containing species capable of the oxidative removal of CO and CH_3CO species adsorbed on adjacent Pt active sites. Adsorption of WO_3 on the catalyst surface can provide additional –OH groups which may participate in electrooxidation of the above mentioned poisoning species. Another possible explanation may take into account so called hydrogen spillover effect and

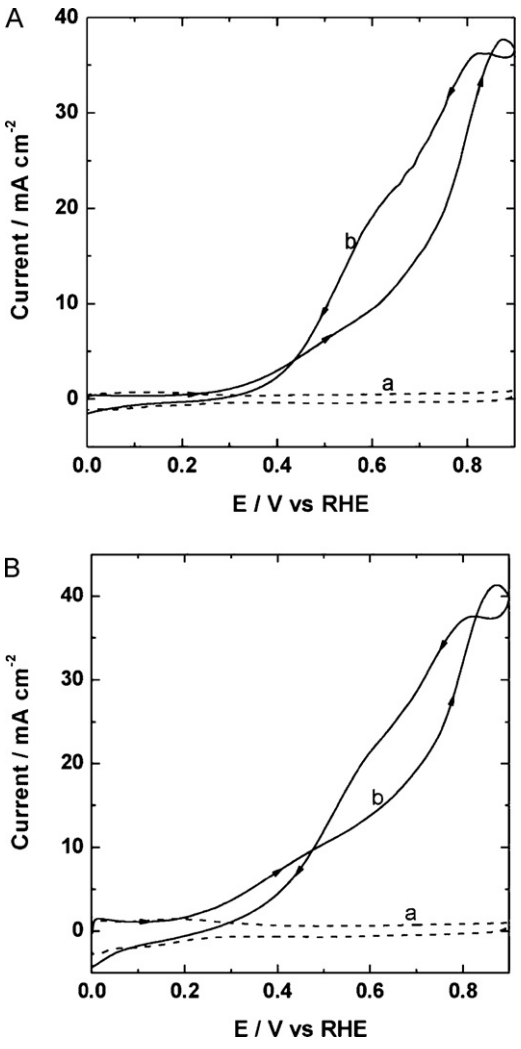

Fig. 5. Cyclic voltammetric responses for oxidation of 0.5 mol dm^{-3} ethanol (curves b) on PtSn/C (A) and WO_3-modifed PtSn/C (B) catalysts. Electrolyte: 0.5 mol dm^{-3} H_2SO_4. Scan rate: 10 mV/s. Curves a show responses in the absence of ethanol.

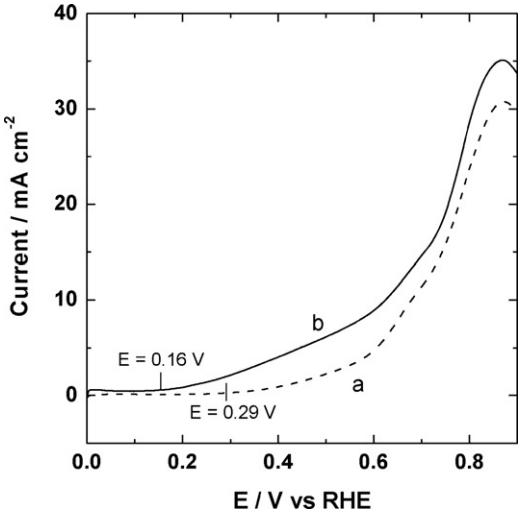

Fig. 6. Linear scan voltammetry responses for oxidation of 0.5 mol dm^{-3} ethanol at PtSn/C (a), and WO_3-modifed PtSn/C (b) catalyst at 10 mV s^{-1} scan rate. Electrolyte: 0.5 mol dm^{-3} H_2SO_4.

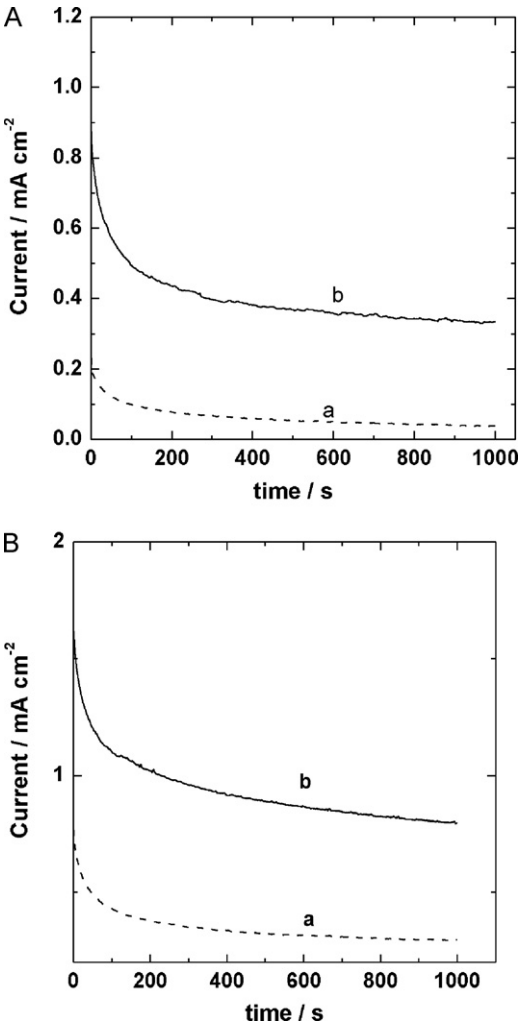

Fig. 7. Chronoamperometric current–time responses (recorded at 0.3 V (A), and 0.4 V (B)) for oxidation of 0.5 mol dm^{-3} ethanol at bare PtSn/C (a), and WO_3-modifed PtSn/C (b) catalysts. Electrolyte: 0.5 mol dm^{-3} H_2SO_4. Scan rate: 10 mV/s.

specific interactions with platinum sites affecting their electronic and adsorptive properties.

It was also reported for tri-metallic PtRu-W systems that addition of tungsten in the vicinity of platinum led to increase its catalytic activity of towards electrooxidation of ethanol in comparison to simple bimetallic PtRu catalysts [26,51]. It was not specified whether the presence of tungsten increased activity of ruthenium (according to well-known bifuctional mechanism [26,51] or specific interactions existing between platinum and tungsten resulted in interfacial electronic changes affecting the force of adsorption of passivating residues on platinum [52].

In order to obtain more information about electrocatalytic activity of the investigated systems, chronoamperometric measurements (Fig. 7) were performed at three different potentials; 0.3 V, 0.4 V and 0.45 V (for simplicity, chronoamperogram for the latter potential is not shown here), and the currents were normalized against the electrode surface area. The modification of PtSn/C nanoparticles with WO_3 leads to the evident increases of catalytic currents under chronoamperometric conditions (compare dotted and solid lines in Fig. 7A and B). As expected from the voltammetric data (Fig. 5), the enhancement effect has been the most pronounced for WO_3-modifed PtSn/C nanoparticles. There is a sharp decrease in the current density during the initial stage, followed by a slow decrease over longer periods of time. At the beginning the active

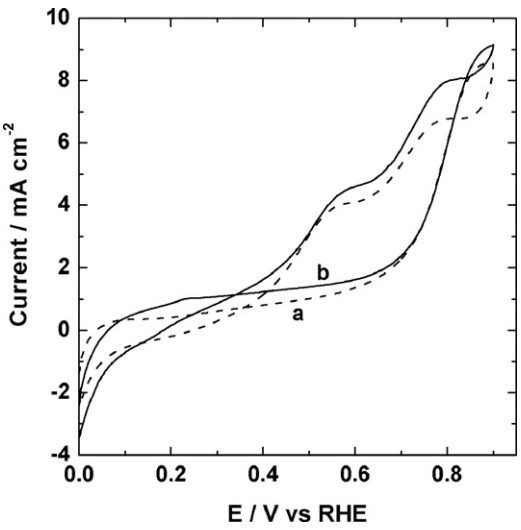

Fig. 8. Cyclic voltammetric responses of oxidation of 0.25 mol dm^{-3} acetaldehyde on PtSn/C (a), and WO_3-modifed PtSn/C (b) catalysts. Electrolyte: 0.5 mol dm^{-3} H_2SO_4. Scan rate: 10 mV/s.

sites are free of adsorbed ethanol molecules (fast kinetic rate reaction); after that, the adsorption of new ethanol molecules is a function of the liberation of the active sites by ethanol oxidation or intermediate species, such as CO, CH_x, CH_3CHO and CH_3COOH formed during the first minutes (rate determining step) [53] that are responsible for poisoning of the catalytic sites.

To comment on prolonged stability of the electrocatalytic responses in the presence of ethanol, the long-term chronoamperometric measurements of WO_3- modified PtSn/C system have been performed (not show here) under conditions of Fig. 7. Following initial sizable decay occurring within first 120 s, further chronoamperometric experimentation for 1 h results only in 15% decrease of catalytic currents when the modified system (rather than bare nanoparticles) has been used.

3.4. Electro-oxidation of acetaldehyde and acetic acid

One of the major intermediate products of oxidation of ethanol is acetaldehyde. We have performed comparative voltammetric experiments to investigate oxidation of acetaldehyde over the two, bare PtSn/C and WO_3-modifed PtSn/C, catalysts. The respective voltammetric curves recorded under the same conditions in 0.25 mol dm^{-3} CH_3CHO + 0.5 mol dm^{-3} H_2SO_4 are shown in Fig. 8. It is not surprising that, in cases of both catalysts, hydrogen surface peaks characteristic of clean platinum surface are largely suppressed by adsorbed acetaldehyde. Electrooxidation of acetaldehyde seem to proceed more effectively at WO_3-modifed PtSn/C catalysts both in terms of higher currents and the lower onset oxidation potential (Fig. 8). It is apparent that some oxidative decomposition of acetaldehyde occurs at WO_3-modifed PtSn/C (but not at bare PtSn/C) at potentials lower than 0.3 V. Because acetaldehyde is a side product of the oxidation of ethanol, it is reasonable to expect higher oxidation currents in the case of WO_3-modifed PtSn/C (see Figs. 5 and 7). Finally none of the catalytic systems studied here has been practically active towards acetic acid oxidation (Fig. 9) in the investigated range of potentials. Apparently, acetic acid (rather than carbon dioxide) is a predominant final product of ethanol oxidation even when WO_3-modifed PtSn/C has been utilized (despite the fact that the latter system is elecrocatalytically more efficient). Further research is necessary to develop catalytic systems capable of more effective C–C bond breaking.

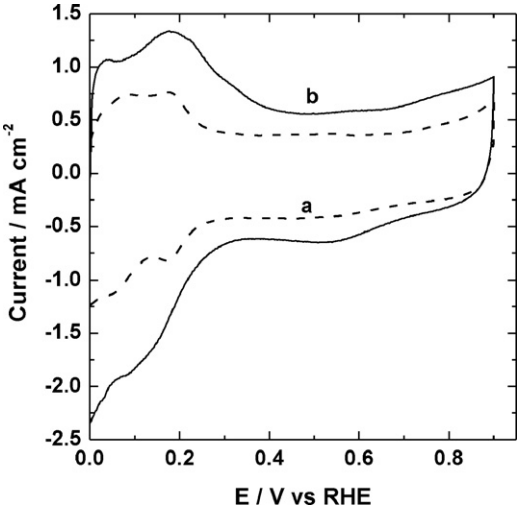

Fig. 9. Cyclic voltammetric responses for oxidation of 0.25 mol dm^{-3} acetic acid on PtSn/C (a) and WO_3-modifed PtSn/C (b) catalysts. Basic electrolyte: 0.5 mol dm^{-3} H_2SO_4. Scan rate: 10 mV/s.

4. Conclusions

We demonstrate here the activating role of tungsten oxide on PtSn/C towards electrooxidation of ethanol and its intermediate by-product, acetaldehyde. In the presence of ultra-thin layers of WO_3, PtSn/C nanoparticles yield higher catalytic currents both under voltammetric and chronoamperometric conditions. The activation effect may involve direct specific interactions between WO_3 and Pt sites. By analogy to the recently reported activating role of polyoxometallates on Pt-based catalysts [52], chemical, electronic and stabilizing interactions of tungsten oxide with tin or tin oxo species can be expected. WO_3 may also provide –OH groups and thus participate in removing of poisoning species from the catalytic surface.

Acknowledgements

This work was supported by Ministry of Science and Higher Education (Poland) under the Singapore/112/2007 collaborative project. K.M. was partially supported by the University of Warsaw under grant BW-179212. The support from Foundation for Polish Science (FNP) under Chair (*Mistrz*) Program is highly appreciated.

References

[1] J.P.I. de Souza, S.L. Queiroz, K. Bergamaski, E.R. Gonzalez, F.C. Nart, J. Phys. Chem. B 106 (2002) 9825.
[2] S.-C. Chang, L.-W.H. Leung, M.J. Weaver, J. Phys. Chem. 94 (1990) 6013.
[3] T. Iwasita, J. Braz. Chem. Soc. 13 (2002) 401.
[4] P.J. Barczuk, A. Lewera, K. Miecznikowski, P.J. Kulesza, J. Augustynski, Electrochem. Solid-State Lett. 12 (2009) B165.
[5] M. Heinen, Z. Jusys, R.J. Bhem, J. Phys. Chem. C 114 (2010) 9850.
[6] V.M. Schmidt, R. Ianniello, E. Pastor, S.R. Gonz_alez, J. Phys. Chem. 100 (1996) 17901.
[7] T. Iwasita, E. Pastor, Electrochim. Acta 39 (1994) 531.
[8] X.H. Xia, H.-D. Liess, T. Iwasita, J. Electroanal. Chem. 437 (1997) 233.
[9] F. Delime, J.-M. Lĩeger, C. Lamy, J. Appl. Electrochem. 29 (1999) 1249.
[10] G. Tremiliosi-Filho, H. Kim, W. Chrzanowski, A. Wieckowski, B. Grzybowska, P. Kulesza, J. Electroanal. Chem. 467 (1999) 143.
[11] M. Watanabe, S. Motoo, J. Electroanal. Chem. 60 (1975) 259.
[12] A. Hamnett, Interfacial Electrochemistry – Theory Experiment and Applications, Marcel Dekker, New York, 1999, Chapter 47, pp. 871–873.
[13] H.A. Gasteiger, N. Markovic, P.N. Ross, E.J. Cairns, J. Phys. Chem. 97 (1993) 12020.
[14] A. Oliveira Neto, R.R. Dias, Marcelo M. Tusi, M. Linardi, E.V. Spinacé, J. Power Sources 166 (2007) 87.
[15] S.Q. Song, W.J. Zhou, Z.H. Zhou, L.H. Jiang, G.Q. Sun, Q. Xin, V. Leontidis, S. Kontou, P. Tsiakaras, Int. J. Hydrogen Energy 30 (2005) 995.
[16] J. Mann, Nan Yao, A.B. Bocarsly, Langmuir 22 (2006) 10432.
[17] J.-M. Léger, S. Rousseau, C. Coutanceau, F. Hahn, C. Lamy, Electrochim. Acta 50 (2005) 5118.
[18] A. Kowal, M. Li, M. Shao, K. Sasaki, M.B. Vukmirovic, J. Zhang, N.S. Marinkovic, P. Liu, A.I. Frenkel, R.R. Adzie, Nat. Mater. 8 (2009) 325.
[19] A. Kowal, S.Lj. Gojkovic, K.-S. Lee, P. Olszewski, Y.-E. Sung, Electrochem. Commun. 11 (2009) 724.
[20] E. Antolini, J. Power Sources 170 (2007) 1.
[21] G.A. Camara, R.B. de Lima, T. Iwasita, Electrochem. Commun. 6 (2004) 812.
[22] V. Pacheco Santos, V. Del Colle, R. Batista de Lima, G. Tremiliosi-Filho, Langmuir 20 (2004) 11064.
[23] J. Ribeiro, D.M. dos Anjos, K.B. Kokoh, C. Coutanceau, J.-M. Leger, P. Olivi, A.R. de Andrade, G. Tremiliosi-Filho, Electrochim. Acta 52 (2007) 6997.
[24] J. Ribeiro, D.M. dos Anjos, J.-M. Leger, F. Hahn, P. Olivi, A.R. de Andrade, G. Tremiliosi-Filho, K.B. Kokoh, J. Appl. Electrochem. 38 (2008) 653.
[25] D.M. dos Anjos, F. Hahn, J.-M. Leger, K.B. Kokoh, G. Tremiliosi-Filho, J. Braz. Chem. Soc. 19 (2008) 795.
[26] S. Tanaka, M. Umeda, H. Ojima, Y. Usuń, O. Kimura, I. Uchida, J. Power Sources 152 (2005) 34.
[27] P.J. Kulesza, L.R. Faulkner, J. Electroanal. Chem. 259 (1989) 81.
[28] P.J. Kulesza, L.R. Faulkner, J. Am. Chem. Soc. 110 (1988) 4905.
[29] P.J. Kulesza, L.R. Faulkner, J. Electroanal. Chem. 248 (1988) 305.
[30] J.-F. Roland, F.C. Anson, J. Electroanal. Chem. 336 (1992) 245.
[31] P.J. Kulesza, L.R. Faulkner, Colloids Surf. 41 (1989) 123.
[32] P.K. Shen, A.C.C. Tseung, J. Electrochem. Soc. 141 (1994) 3082.
[33] M. Umeda, H. Ojima, M. Mohamedi, I. Uchida, J. Power Sources 136 (2004) 10.
[34] P.J. Weisman, P.G. Dickens, J. Solid State Chem. 6 (1973) 374.
[35] B.S. Hobbs, A.C.C. Tseung, J. Electrochem. Soc. 122 (1975) 1174.
[36] R.S.S. Crandall, B.W. Faughnan, Appl. Phys. Lett. 28 (1976) 95.
[37] P.J. Kulesza, L.R. Faulkner, J. Electrochem. Soc. 136 (1989) 707.
[38] L.W. Niedrach, H.I. Ziegler, J. Electrochem. Soc. 116 (1969) 152.
[39] L.X. Yang, C. Bock, B. MacDougall, J. Park, J. Appl. Electrochem. 34 (2004) 427.
[40] J. Shim, C.-R. Lee, H.-K. Lee, J.-S. Lee, E.J. Cairns, J. Power Sources 102 (2001) 172.
[41] H. Wang, Z. Jusys, R.J. Behm, J. Phys. Chem. B 108 (2004) 19413.
[42] Z. Jusys, J. Kaiser, R.J. Behm, Langmuir 19 (2003) 6759.
[43] A. Manzo-Robledo, A.-C. Boucher, E. Pastor, N. Alsono-Vante, Fuel Cells 2 (2002) 109.
[44] L. Jiang, L. Colmenares, Z. Jusys, G.Q. Sun, R.J. Behm, Electrochim. Acta 53 (2007) 377.
[45] B.N. Grgur, N.M. Markovic, P.N. Ross, J. Phys. Chem. B 102 (1998) 2494.
[46] K. Wang, H.A. Gasteiger, N.M. Markovic, P.N. Ross, Electrochim. Acta 41 (1996) 2587.
[47] T.J. Schmidt, H.A. Gasteiger, R.J. Behm, J. New Mater. Electrochem. Syst. 2 (1999) 27.
[48] M.M. Schubert, M.J. Kahlich, G. Feldmeyer, M. Huttner, S. Hackenberg, H.A. Gasteiger, R.J. Behm, Phys. Chem. Chem. Phys. 3 (2001) 1123.
[49] C. Lamy, S. Rousseau, E.M. Belgsir, C. Coutanceau, J.-M. Leger, Electrochim. Acta 49 (2004) 3901.
[50] G.S. Jiang, S. Sun, J. Liu, S. Tang, H. Li, B. Zhou, Q. Xin, Electrochim. Acta 50 (2005) 5384.
[51] W. Zhou, Z. Zhou, S. Song, W. Li, G. Sun, P. Tsiakaras, Q. Xin, Appl. Catal. B 46 (2003) 273.
[52] P.J. Barczuk, A. Lewera, K. Miecznikowski, P.J. Kulesza, J. Power Sources 195 (2010) 2507.
[53] E. Antolini, Appl. Catal., B Environ. 74 (2007) 337.